Drug Delivery and Translational Research (2024) 14:158–176
https://doi.org/10.1007/s13346-023-01390-z

ORIGINAL ARTICLE

Sirolimus-loaded exosomes as a promising vascular delivery system for the prevention of post-angioplasty restenosis

Fatemeh Mehryab[1] · Shahram Rabbani[2] · Faezeh Shekari[3] · Abdoreza Nazari[3] · Nazanin Goshtasbi[1] · Azadeh Haeri[1,4]

Accepted: 11 July 2023 / Published online: 30 July 2023

Abstract

Restenosis remains the main reason for treatment failure of arterial disease. Sirolimus (SIR) as a potent anti-proliferative agent is believed to prevent the phenomenon. The application of exosomes provides an extended-release delivery platform for SIR intramural administration. Herein, SIR was loaded into fibroblast-derived exosomes isolated by ultracentrifugation. Different parameters affecting drug loading were optimized, and exosome samples were characterized regarding physicochemical, pharmaceutical, and biological properties. Cytotoxicity, scratch wound assays, and quantitative real-time PCR for inflammation- and migration-associated genes were performed. Restenosis was induced by carotid injury in a rat carotid model and then exosomes were locally administered. After 14 days, animals were investigated by computed tomography (CT) angiography, morphometric, and immunohistochemical analyses. Western blotting confirmed the presence of specific protein markers in exosomes. Characterization of empty and SIR-loaded exosomes verified round and nanoscale structure of vesicles. Among prepared formulations, desired entrapment efficiency (EE) of 76% was achieved by protein:drug proportion of 2:1 and simple incubation for 30 min at 37 °C. Also, the optimal formulation released about 30% of the drug content during the first 24 h, followed by a prolonged release for several days. In vitro studies revealed the uptake and functional efficacy of the optimized formulation. In vivo studies revealed that %restenosis was in the following order: saline > empty exosomes > SIR-loaded exosomes. Furthermore, Ki67, alpha smooth muscle actin (α-SMA), and matrix metalloproteinase (MMP) markers were less expressed in the SIR-exosomes-treated arteries. These findings confirmed that exosomal SIR could be a hopeful strategy for the prevention of restenosis.

Keywords Exosomes · Extracellular vesicles · Sirolimus · Restenosis · Balloon angioplasty

Introduction

Cardiovascular disease is a major cause of mortality globally. The atherosclerotic plaques' formation is the starting point of many cardiovascular diseases. It commonly affects carotid and coronary arteries and leads to stenosis or obstruction of vessels and occasionally an ischemic stroke [1, 2]. The main therapeutic strategies include percutaneous coronary interventions and surgical revascularization. Different percutaneous coronary intervention approaches have been applied such as balloon angioplasty and the application of bare-metal (BMS) and drug-eluting stents (DES) [3]. Several problems were reported regarding stenting such as late thrombosis, limited use in branched vessels, permanent remaining of stents, and the increased risk of in-stent restenosis [4].

✉ Azadeh Haeri
a_haeri@sbmu.ac.ir

1 Department of Pharmaceutics and Pharmaceutical Nanotechnology, School of Pharmacy, Shahid Beheshti University of Medical Sciences, PO Box: 14155-6153, Tehran, Iran

2 Research Center for Advanced Technologies in Cardiovascular Medicine, Cardiovascular Diseases Research Institute, Tehran University of Medical Sciences, Tehran, Iran

3 Department of Stem Cells and Developmental Biology, Cell Science Research Center, Royan Institute for Stem Cell Biology and Technology, ACECR, Tehran, Iran

4 Protein Technology Research Center, Shahid Beheshti University of Medical Sciences, Tehran, Iran

A possible solution is the use of drug-coated balloons (DCB), and to improve the efficacy of DCB, some studies aimed to coat balloons with drug nanocrystals and exhibited superior healing features [5, 6]. In addition, drug-loaded nanoparticles can be applied to further sustain the drug release at the target site [7]. Accordingly, the application of drug-loaded nanoparticles in combination with balloon angioplasty and/or stenting was considered a promising approach [8]. The idea of balloon angioplasty, followed by the local delivery of anti-restenosis nanodrugs is another recent solution to answer the limitations of previous therapeutic approaches [7, 8]. By this approach, some nanostructures such as liposomes [7], micelles [9], phospholipidic nanoparticles [10], and polymeric nanoparticles [11] were investigated by our team and other researchers for the sustained intramural delivery of desired hydrophobic drugs to the affected arteries.

Exosomes are a new class of delivery nanosystems that originated from almost all cells. These natural vesicles are present in body fluids and have an intercellular communication role [12–17]. They also contain a parental cargo that can modulate immune responses [13, 18]. They may be isolated from the culture medium of stem cells and applied as biocompatible nanocarriers [16, 19, 20]. Fibroblasts serve a common cellular origin previously investigated in pre-clinical and clinical studies of cell therapy. They benefit from stem cell properties and carry a specific marker that protects vesicles from phagocytic uptake resulting in a long circulation half-life [21, 22].

Sirolimus (SIR), also known as rapamycin, is a macrolide antibiotic that is used as an immunosuppressant drug in clinics [1, 23]. It inhibits the mammalian target of rapamycin (mTOR) involved in many cellular processes including growth, proliferation, angiogenesis, autophagy, lymphangiogenesis, and several metabolic reactions [24]. It is used in the prevention of organ transplant rejection and as an adjuvant treatment in chemotherapy regimens [23]. It is also used in several vascular anomalies discussed widely elsewhere [24, 25]. Due to anti-inflammatory and proliferative activities, SIR is used for the design of DES and DCB to prevent restenosis [3]. Overall, SIR can be a promising agent for the prevention of restenosis in arteries undergoing balloon angioplasty [7].

Motivated by this rationale, the present study was focused on the application of SIR-loaded exosomes (SIR-EXO) for intramural local drug delivery (Fig. 1). In this study, SIR molecules were incorporated into fibroblast-derived exosomes by different loading strategies, and the optimal formulation was characterized regarding the exosomal identity, entrapment efficiency (EE), size, morphology, and release profile. Exosome samples were further studied regarding biocompatibility, cytotoxicity against smooth muscle cells (SMCs), scratch wound assays, cellular uptake, and quantitative real-time polymerase chain reaction (PCR) for inflammation- and migration-associated genes including interleukin-1 beta (IL-1β), tumor necrosis factor alpha (TNF-α), and matrix metalloproteinase-2

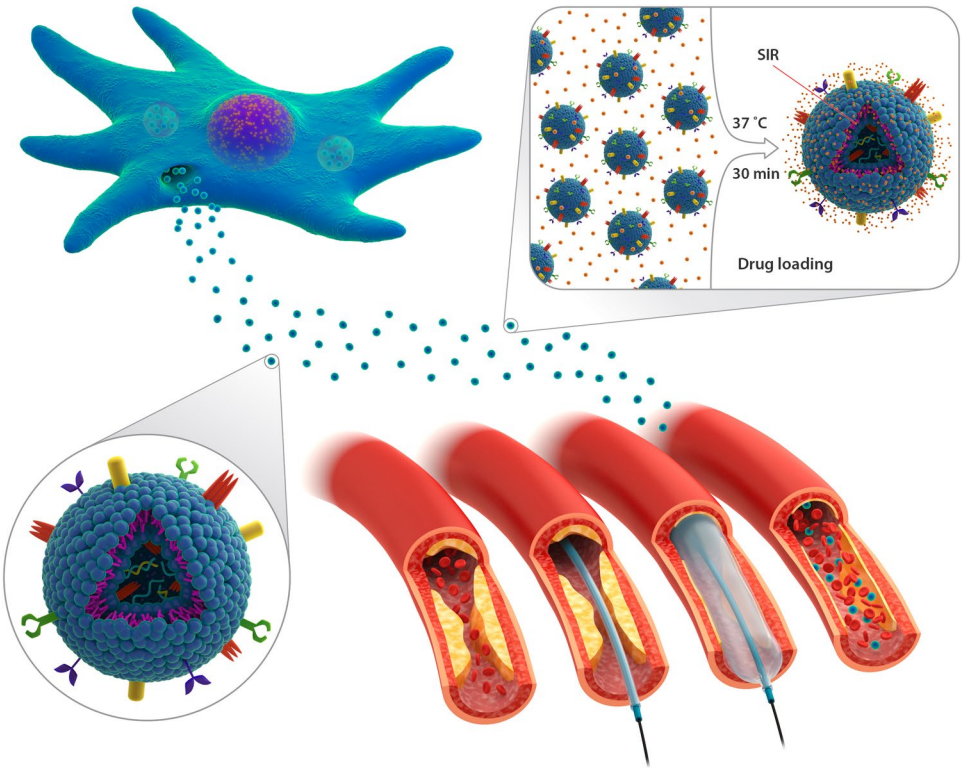

Fig. 1 An illustration of exosome production by fibroblast cells, drug loading into vesicles, and local delivery of exosomal SIR in the injured carotid artery

(MMP-2). Moreover, SIR-EXO and empty exosomes (Empty-EXO) were administered locally after balloon angioplasty in a rat model for the prevention of restenosis. The efficacy of the proposed nanoformulation was investigated by relevant experiments.

Materials and methods

Materials

SIR powder (98% purity) was acquired from Fujian Kerui Pharmaceutical Co., Ltd. (China). Dimethyl sulfoxide (DMSO), ethanol, acetonitrile, methanol, sodium chloride, and Tween 80 were obtained from Merck KGaA (Germany).

Cell culture

Human fibroblasts (Royan Institute, Iran) were cultured in fetal bovine serum (FBS; Gibco, Germany) supplemented Dulbecco's modified Eagle's medium (DMEM; Gibco, Germany). At 70% confluence, a fresh medium supplemented with exosome-depleted FBS was replaced. After 48 h, the conditioned medium was pooled for the purification of exosomes.

SMCs were obtained by the differentiation of human embryonic stem cells (hESCs) (Royan Institute, Iran). The stem cells were cultured in Dulbecco's modified Eagle's medium/Ham's F-12 (DMEM/F12; Gibco, Germany) containing 20% serum replacement (Gibco, Germany), 0.1 mM β-mercaptoethanol (Merck KGaA, Germany), 100 ng/mL basic fibroblast growth factor (bFGF; Royan Biotech, Iran), 1% insulin-transferrin-selenite (Gibco, Germany), and 1% nonessential amino acids (NEAA; Gibco, Germany). The medium was conditioned overnight on mitomycin C (Merck KGaA, Germany) inactivated fibroblasts and then used for the formation of hESCs spheroids in non-adhesive culture plates. Cells were incubated with 10 μM of Rho-kinase inhibitor (Merck KGaA, Germany) for 48 h, and then the medium was refreshed every 2 days. For the induction of hESCs into cardiomyocytes, cell spheroids were incubated with 12 μM of CHIR99021 (Abcam, UK) in Roswell Park Memorial Institute (RPMI-1640; Gibco, Germany) containing 2% B-27 supplement (minus vitamin A; Gibco, Germany), 2 mM L-glutamine (Gibco, Germany), 0.1 mM β-mercaptoethanol, and 1% NEAA for 24 h and then cultured without small molecules for another 24 h as described earlier [26].

Then, spheroids were dissociated into singular cells by Accutase (Merck KGaA, Germany), and cells were cultured in the supplemented DMEM/F12 containing 0.5 μM A83-01 (Abcam, UK), 100 ng/mL fresh bFGF, and 3 μM CHIR99021 on Matrigel-coated plates, and this maintenance medium was replaced daily. Afterward, cardiomyocytes were cultured in a differentiation medium containing 5 μM purmorphamine (Merck KGaA, Germany), 5 μM IWP2 (Merck KGaA, Germany), and 5 μM SB431542 (Merck KGaA, Germany) for 48 h. Then, cells were cultured in a maintenance medium supplemented with transforming growth factor-beta 1 (TGF-β1; Merck KGaA, Germany) and platelet-derived growth factor-BB (PDGF-BB; Merck KGaA, Germany) for 12 days to differentiate into SMCs. The medium was refreshed every 72 h.

Exosomes purification

Exosomes were isolated from the conditioned medium by the ultracentrifugation method introduced by Thery et al. [27] with minor modifications. Briefly, the pooled medium was centrifuged at 350 g to pellet cells. The supernatant was then centrifuged at 3000 g to remove debris and the remaining supernatant was ultracentrifuged by a 45 Ti rotor (Beckman Coulter Life Sciences, USA) at 20,000 g for 30 min resulting in the formation of a pellet of microvesicles. The obtained supernatant was ultracentrifuged at 110,000 g for 120 min, and exosomes were pelleted. The pellet was dispersed in 1 mL normal saline (NS) and again pelleted at 110,000 g and the packed exosomes were suspended in NS and stored at − 80 °C.

Characterization of Empty-EXO

Identification

The protein content of exosomes was quantified by Bradford reagent (Merck KGaA, Germany), followed by western blotting to verify the presence of exosomal markers, as described earlier [28]. Initially, the protein samples were incubated at 95 °C for 10 min and then sonicated for 5 min. Proteins of different samples were separated by sodium dodecyl sulfate–polyacrylamide gel electrophoresis (SDS-PAGE) and then transferred to a polyvinylidene fluoride (PVDF) membrane. The membrane was blocked and incubated with CD63 (Santa Cruz Biotechnology, Germany), CD81 (Santa Cruz Biotechnology, Germany), and tumor susceptibility gene 101 (TSG101; Genetex, Germany) antibodies as positive markers and Calnexin (Santa Cruz Biotechnology, Germany) antibody as a negative marker. After incubation with primary antibodies, the membrane was incubated with a secondary antibody. After washing, enhanced chemiluminescence (ECL) substrate was added to the blot, and the blot was imaged by a gel documentation system (Uvitec Ltd., UK).

Size distribution and surface charge

For measurement of the vesicles' mean diameter and zeta potential, 10–20 µL exosomes (1 mg/mL) were diluted in 1 mL distilled water. The sample was measured by a Zetasizer (Malvern Instruments, UK) and analyzed regarding the mean diameter, polydispersity index (PDI), and surface charge.

Morphology studies

The morphology of vesicles was studied by transmission electron microscopy (TEM), atomic force microscopy (AFM), and scanning electron microscopy (SEM). A drop of each sample was loaded on a carbon-coated copper grid, stained with a drop of uranyl acetate (Agar Scientific, UK), and then the grid was allowed to be air-dried. Imaging was carried out by an EM10C instrument (Zeiss, Germany) at an accelerating 100 kV voltage.

For AFM observation, a drop of each diluted sample was placed on a slide and air-dried. The topography of exosomes was studied and imaged by AFM (NanoWizard II; JPK Instruments, Germany) using a silicon cantilever in the contact mode. Obtained data were further studied and processed by JPK software (JPK Instruments, Germany).

For SEM observation, a drop of diluted exosomes was placed on a coverslip and air-dried. Then, samples were coated with gold by Desk Sputter Coater DSR1 (NanoStructured Coatings Co., Iran) and imaged by MIRA3 (TESCAN, Czech Republic).

Drug loading of exosomes

Exosomes were mixed with SIR solution and different loading methods, duration, and drug-to-protein ratios were investigated to optimize the drug loading. First, simple incubation at 37 °C was studied for 30 and 60 min. Thereafter, electroporation and sonication were used after incubation. Briefly, sonication was performed for 6 cycles (30 s on and 2 min off) using a sonicator (Liarre, Italy). Electroporation was performed by a multiporator (Eppendorf, Germany) at 500 V, and two pulses were made with a duration of 5 ms and a 30-s interval between pulses. To load exosomes by a new approach, a thin SIR film was formed by the drug solution evaporation in a microtube, and exosomes were added to the tube. The mixture was sonicated for 10 min, and then vesicles were annealed at room temperature for 30 min.

Characterization of SIR-EXO

SIR-EXO were characterized by western blotting to verify the stability of the specific markers of exosomes during the loading process. Size distribution, PDI, and zeta potential of SIR formulations were studied and compared with Empty-EXO. Moreover, morphology studies including TEM, AFM, and SEM were performed for the optimized SIR-EXO, and obtained data were compared with intact vesicles.

Entrapment efficiency (EE)

The free drug was isolated using centrifugation at 14,000 rpm for 10 min and separated at the bottom of the microtube. Exosomes were digested with methanol, and the mixture was vortexed vigorously. SIR concentration was measured using a validated high-performance liquid chromatography (HPLC) method [7]. EE was calculated by the following equation:

$$\text{EE}\ (\%) = \text{incorporated drug amount} \times 100 \,/\, \text{added drug amount}$$

Drug release profile

Drug release study of the optimized SIR-EXO was carried out by dialysis membrane (12 kDa cut-off). NS containing 0.05% (w/v) Tween 80 was chosen as the release medium to provide sink conditions. Each sample (0.3 mL) was transferred to a dialysis bag and placed in the release medium at 37 °C with shaking at 100 RPM. Sampling was carried out at 1, 2, 4, 6, 8, 10, 24 h, and then every 24 h for 3 weeks. The release medium was replaced daily, and samples were analyzed using HPLC as described earlier [7]. The experiment was performed in triplicate and obtained data were evaluated regarding different probable equations including zero order, first order, and Higuchi [29]. The best model was selected following comparisons among obtained correlation coefficients.

Fourier-transform infrared spectroscopy (FTIR)

For FTIR analysis, a drop of each sample (SIR, Empty-EXO, and SIR-EXO) was deposited on a ZnSe disc and air-dried. The spectrum was obtained in an inert atmosphere at a resolution of 4 cm^{-1} over a wavenumber range of 600–4000 cm^{-1} by a WQF-510 laboratory FTIR spectrometer (Beijing Rayleigh Analytical Instrument Corporation, China).

Hemolysis test

The hemolysis test was carried out according to ISO 10993–4:2002 as described earlier [30]. A fresh rat blood sample was mixed with 10 mL NS and then centrifuged at 3000 RPM for 10 min. After discarding the supernatant, the obtained pellet was washed and packed erythrocytes were dispersed in NS to obtain a 2% (w/v) suspension. Different samples of SIR-EXO, Empty-EXO, and SIR suspension (characterized regarding its particle size and zeta potential

(Table S1, Fig. S1)) were mixed with erythrocyte suspension and incubated at 37 °C for 120 min. Deionized water and NS were applied as positive and negative control samples, respectively. Samples were centrifuged, and the supernatants' absorbance was measured at 545 nm. Hemolysis was evaluated by the formula:

$$\text{Hemolysis}\ (\%) = (\text{absorbance}_{\text{test sample}} - \text{absorbance}_{\text{negative control}}) \times 100 / (\text{absorbance}_{\text{positive control}} - \text{absorbance}_{\text{negative control}})$$

The sample was interpreted as hemolytic if the hemolysis (%) was observed higher than 5%.

In vitro studies

Cellular uptake

SMCs were incubated with a drug suspension and SIR-EXO with 5000 and 200 ng/mL SIR for 3 and 24 h, respectively. Then, the medium was discarded and cells were gently washed, detached, and dispersed in NS. Cell suspensions were digested using methanol, and then the SIR concentration was measured by the HPLC.

MTT assay

Differentiated SMCs were cultured in Matrigel-coated flat bottom 96-well plates (10^4 cells/well) overnight. Then, SMCs were treated with different doses of free and loaded SIR for 48 h. Afterward, 20 µL 3-(4,5-dimethylthiazol-2-yl)-2,5-diphenyl-2H-tetrazolium bromide (MTT) reagent was added to each well, and the plate was read at 570 nm.

Quantitative real-time polymerase chain reaction (PCR)

Cellular total RNA was extracted using TRIzol reagent, and its quantity and quality were evaluated by a WPA Biowave II UV/Visible Spectrophotometer (Biochrom Ltd., UK) and gel electrophoresis, respectively. Then, cDNA samples were synthesized using a cDNA Synthesis Kit (Parstous, Iran). Primers were acquired from Royan Institute (Iran), and the SYBR Green master mix (Qiagen, Germany) was applied for the quantitative real-time PCR on StepOnePlus PCR system (Applied Biosystems, US). The GAPDH gene was considered as the internal reference, and the relative expression levels of IL-1β, TNF-α, and MMP-2 mRNAs were determined based on the $2^{-\Delta\Delta CT}$ method.

Scratch wound assay

SMCs were cultured in Matrigel-coated 12-well plates (10^5/well) until fully confluent. Thereafter, the cell monolayer of each well was scratched using a P100 pipette tip. Wells were gently washed to remove detached cells. Then, scratched wells were incubated by culture media of DMEM/F12 supplemented with B-27 (minus vitamin A) containing 5 µg/mL free and loaded SIR and the equivalent amount of Empty-EXO. Wells were imaged by a CKX41 inverted microscope (Olympus) at 4× and 10× magnifications at 6, 24, and 72 h after scratching. The wound closure was calculated as follows: (wound area (0 h) − wound area (*n* h))/wound area (0 h) × 100.

Animal studies

Animals

Male Sprague–Dawley rats weighing 380 ± 20 g were maintained on a regular diet and under standard environmental conditions.

Balloon angioplasty injury and exosomes administration

Vascular injury was induced by the inflation of a balloon catheter introduced to the left common carotid. Rats were anesthetized with an intramuscular administration of medetomidine hydrochloride (1 mg/mL) and ketamine (50 mg/mL) and a 2-French embolectomy balloon catheter was pushed into the common carotid artery through a cut on the external carotid artery. The inflated balloon was passed through the artery, withdrawn, and reintroduced two more times to cause vascular injury. Animals were randomly divided into three groups: (1) SIR-EXO, (2) Empty-EXO, and (3) NS as control ($n = 6$ per group). After the local delivery (equivalent to 100 µg SIR and/or 265 µg protein of exosomes) for 15 min, the external carotid was closed, the normal flow was restored, and the animal was recovered.

Computed tomography (CT) angiography

For in vivo vascular imaging, rats were anesthetized at 2 weeks post-injury, and the tail vein was catheterized for the administration of a contrast agent. Iopamidol (Scanlux®) was intravenously administered at a 0.1 mL s^{-1} flow rate, and the exposure parameter and effective current were adjusted to 80 kV and 80 mAs. Obtained results were transferred to the Syngo X Workplace (Siemens, Germany).

Histological analysis

Two weeks post-injury, animals were sacrificed and carotid arteries were perfused in vivo with saline and then fixed

with the continuous perfusion of 10% buffered formalin. Then, left common carotid arteries were collected at the site of injury, further fixed ex vivo for 48 h, paraffin-embedded, and thereafter sectioned. For each staining, at least two serial cross-sections of each carotid were fixed on a microscope slide and slides were labeled by codes for blinding evaluation. Sections were stained with hematoxylin and eosin (H&E), Masson's trichrome, and Orcein-Giemsa and imaged by a BX51 microscope (Olympus, Japan). Afterward, areas of the internal elastic lamina (IEL), external elastic lamina (EEL), and residual lumen were quantified by ImageJ® software (National Institutes of Health, USA). Neointimal and medial areas were obtained by deduction of the residual lumen from IEL and IEL from EEL areas, respectively. Neointima/media (N/M) ratio and stenosis (%) were compared among the study groups.

Immunohistochemical analysis

Briefly, prepared sections of the carotid artery were deparaffinized and rehydrated. Thereafter, sections were treated with hydrogen peroxide and then boiled in citrate buffer (pH 6.0). Samples were stained with Ki67 (Abcam, UK), smooth muscle actin (α-SMA; Abcam, UK), MMP-2 (Abcam, UK), and MMP-9 (Abcam, UK) antibodies at room temperature for 60 min. After rinsing, sections were treated with secondary antibodies for another 60 min, and detection of the reaction product was carried out by 3, 3-diaminobenzidine (DAB; Abcam, UK) counterstained with hematoxylin. Blinding evaluation was achieved by code-based slide labeling and after imaging of prepared slides, ImageJ® software was used for quantification of the results. In this regard, the density of α-SMA, MMP-2, and MMP-9 was assessed in treated sections and reported as stained area per total area (μm^2). In Ki67 staining, the number of positive over total cells was determined.

Statistical analysis

All data were analyzed by GraphPad Prism 7 (GraphPad Software, USA). Results were expressed as mean ± standard error of the mean (SEM). Furthermore, one-way analysis of variance (ANOVA) with post-comparison tests and *t*-test analyses were performed. $P < 0.05$ was interpreted as significant.

Results

Characterization of Empty-EXO

Fibroblast-derived exosomes were characterized by protein content, exosome-associated proteins, size distribution, charge, and morphology (Fig. 2). Morphology studies confirmed a round and vesicular shape for purified exosomes obtained by TEM, SEM, and AFM analyses (Fig. 2a–c). The results revealed the presence of specific exosomal markers (CD63, CD81, and TSG101) (Fig. 2d, Fig. S2). Empty-EXO showed a mean diameter, PDI, and zeta potential of 152.3 ± 2.3 nm, 0.31 ± 0.05, and − 29.8 ± 0.3 mV, respectively (Fig. 2e, f).

Effects of loading variables on EE

Details and results of drug incorporation procedures are presented in Table 1. Initially, simple incubation was performed on a 2:1 drug/protein ratio for 30 (F1) and 60 (F2) min resulting in EE percentages of 29.5 ± 0.4 and 29.6 ± 0.6. No significant difference was noted between the two incubation periods ($P = 0.858$). Therefore, further loading studies were performed with 30-min incubation (F3-F9). By electroporation (F3) and sonication (F4) after drug-exosomes incubation, EE (%) was elevated to 32.9 ± 0.2 and 34.1 ± 0.7, respectively. None of these loading approaches (F3, F4) showed superiority when compared to each other ($P = 0.142$). Thereafter, two lower drug/protein ratios were tested and the ratio of 1:2 (F6) showed the highest EE and the *P*-value of < 0.001, as compared to the 2:1 ratio. Further modifications (such as film loading or additional sonication) on formulations with 1:2 drug/protein ratio (F7-F9) resulted in less EE compared to F6 (ANOVA $P < 0.001$), and the optimal formulation was achieved by simple incubation at 37 °C for 30 min and drug/protein ratio of 1:2 (F6) with EE (%) of 75.7 ± 2.6.

Characterization of SIR-EXO

Post-loading characterization aims to understand the formulation properties and confirm the preservation of desired formulation characteristics, especially in naturally derived nanocarriers. Therefore, SIR-EXO were evaluated regarding the integrity of their specific protein markers by western blotting (Fig. 2d). Size distribution and surface charge of drug-loaded vesicles are presented in Table 1. The mean diameter increased through the loading process, while zeta potential was not significantly affected ($P > 0.05$). Moreover, morphology studies were carried out for the optimal formulation and the spherical structure of SIR-loaded vesicles was confirmed (Fig. 2a–c).

Drug release profile

SIR-EXO exhibited a drug release of about 30% within the first 10 h, followed by a sustained release profile for several days (Fig. 3a). It was observed that the optimal formulation released about 17, 19, 24, 29, and 32% of the drug content after 1, 2, 8, 10, and 24 h and then released ~ 1% of SIR content per day. The drug release of the optimal formulation

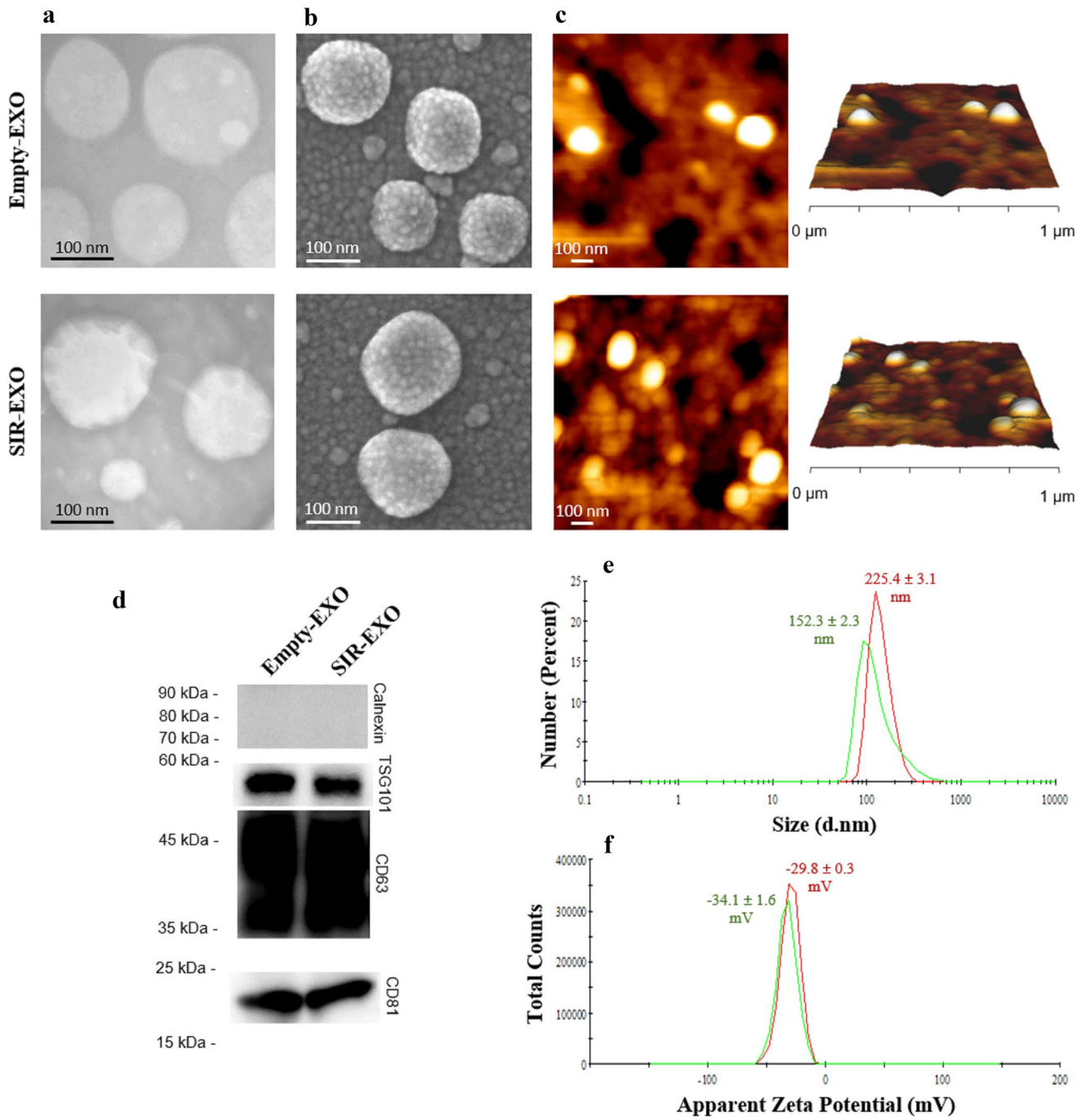

Fig. 2 Characterization studies on exosomes before and after drug loading. **a** TEM, **b** SEM, and **c** AFM images of Empty-EXO and SIR-EXO. **d** Western blot analysis of exosomes before and after loading. **e** Size distribution of Empty-EXO and SIR-EXO. **f** Zeta potential results of Empty-EXO and SIR-EXO

was studied for 3 weeks, and it was observed that exosomes behaved like a depot system and released about half of SIR within 3 weeks.

Further studies on the release profile demonstrated that the average release rate was 1.3%/h in the first 24 h and then gradually decreased to about 1%/day (Fig. 3b). Also, release kinetics was investigated, and data were fitted into different models including zero-order, first-order, and Higuchi models with respective correlation coefficient values of 0.82, 0.87, and 0.93. The model with the highest correlation coefficient was interpreted as the best model for release data. According to statistical analysis, SIR release followed the Higuchi model with the highest correlation coefficient.

Table 1 Summary of drug loading studies and obtained data (mean ± SEM, $n = 3$)

Formulation	Loading details	Drug:protein (weight ratio)	EE[a] (%)	Size after loading (nm)	PDI[b]	Zeta potential (mV)
F1	30 min incubation	2:1	29.5 ± 0.4	228.2 ± 43.4	0.38 ± 0.02	−28.4 ± 0.3
F2	60 min incubation	2:1	29.6 ± 0.6	237.4 ± 35.7	0.36 ± 0.02	−28.7 ± 1.4
F3	30 min incubation + electroporation	2:1	32.9 ± 0.2	360.8 ± 27.5	0.36 ± 0.04	−30.1 ± 0.5
F4	30 min incubation + 3 min sonication	2:1	34.1 ± 0.7	185.2 ± 45.9	0.27 ± 0.01	−29.4 ± 0.4
F5	30 min incubation	1:1	52.6 ± 3.1	243.9 ± 3.6	0.29 ± 0.05	−30.4 ± 1.0
F6	30 min incubation	1:2	75.7 ± 2.6	225.4 ± 3.1	0.31 ± 0.02	−34.1 ± 1.6
F7	Drug film (10 min sonication) + 30 min at RT[c]	1:2	61.3 ± 0.9	247.2 ± 1.6	0.36 ± 0.01	−32.3 ± 0.6
F8	30 min incubation + 3 min sonication	1:2	65.5 ± 0.3	176.0 ± 1.7	0.31 ± 0.02	−31.3 ± 0.4
F9	30 min incubation + 10 min sonication	1:2	73.0 ± 1.1	203.8 ± 9.8	0.39 ± 0.01	−31.5 ± 0.4

[a]*EE* entrapment efficiency, [b]*PDI* polydispersity index, [c]*RT* room temperature

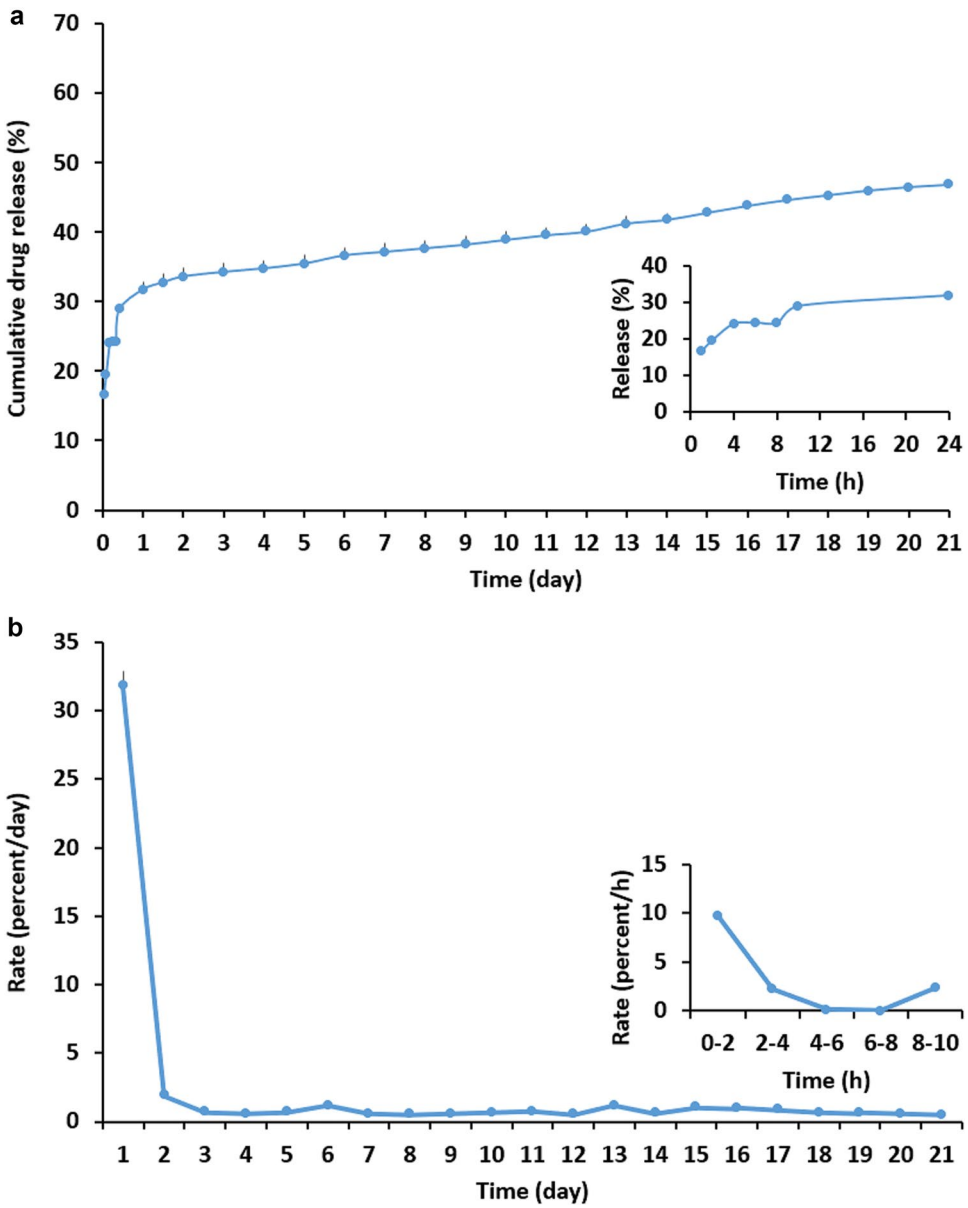

Fig. 3 In vitro drug release **a** profile and **b** rate during 3 weeks of study (mean ± SEM, $n = 3$)

Fourier-transform infrared spectroscopy (FTIR)

FTIR characterization of pure SIR, Empty-EXO, and SIR-EXO was performed to study the interaction of drug molecules with components of exosomes. Characteristic peaks of SIR at 1454, 1649, 1718, 2873, 2933, 2966, and 3018 cm^{-1} were present in the spectrum of pure SIR. Exosomal structure peaks appeared at 1072, 1398, 1539, 1745, 2852, and 2922 cm^{-1} in the Empty-EXO spectrum. Comparing obtained spectra, no significant difference was observed between empty and SIR-loaded exosomes (Fig. 4a).

Hemolysis test

Based on the definition of a hemolytic sample, no hemolysis was observed in all study groups (Fig. 4b, c). Although there was no statistical significance, hemolysis (%) in the SIR-EXO group was lower than SIR group. Also as expected, the Empty-EXO group demonstrated the lowest hemolysis compared to other groups.

In vitro evidence of SIR-EXO efficacy

Differentiated cells were used for the in vitro studies, and for the drug uptake evaluation, SMCs were treated with a low concentration of drug for 24 h to prevent possible toxicity. In a parallel study, a much higher concentration of SIR was used to provide enough drug availability in the conditioned medium of cells, and SMCs were incubated with free SIR and SIR-EXO for 3 h. Cellular uptake of the higher concentration of SIR incubated with SMCs for 3 h was obtained at around 7% in both groups without any significant difference. Also, in both groups incubated with SIR suspension and SIR-EXO for 24 h, about 80% of SIR content was internalized into the cells, and there was no significant difference between the two groups ($P > 0.05$) (Fig. 5a).

Upon the successful uptake of the loaded drug form, further studies were carried out to assess the anti-proliferative and anti-inflammatory effects of SIR-EXO on SMCs, as compared to the free drug. First of all, the MTT assay was performed to determine the anti-proliferative effect of different drug doses on the cells. According to Fig. 5b, considerably similar to the cellular uptake results, free and loaded SIR exhibited similar viability profiles. SIR at even low concentrations could notably reduce cellular viability, and 50 ng/mL loaded SIR resulted in about 50% viability.

Furthermore, the beneficial effects of SIR-EXO on the prevention of inflammation, migration, and invasion were investigated by real-time PCR and wound healing assay. As shown in Fig. 5c, the gene expressions of IL-1β, TNF-α, and MMP-2 were significantly affected by SIR-EXO treatment and down-regulated. The gene expression folds change

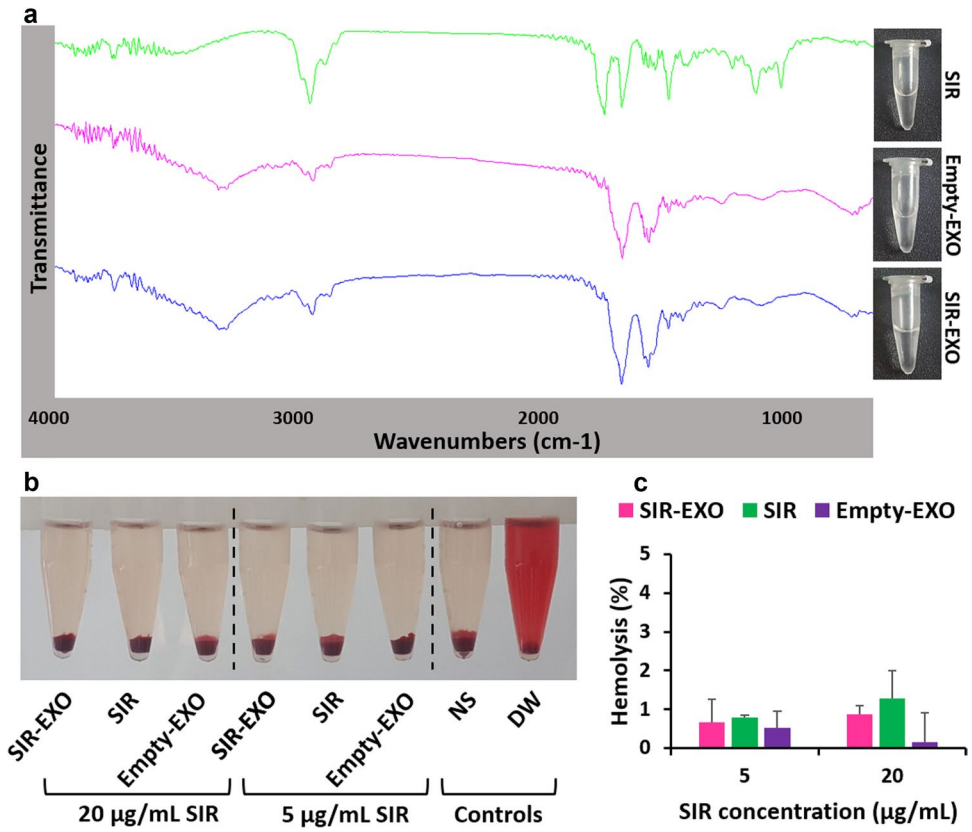

Fig. 4 Obtained results of FTIR and hemolysis studies. **a** FTIR spectra of SIR, Empty-EXO, and SIR-EXO. **b** Photographs of hemolysis samples. **c** Bar chart of hemolysis study; data were reported as mean ± SEM, $n = 3$

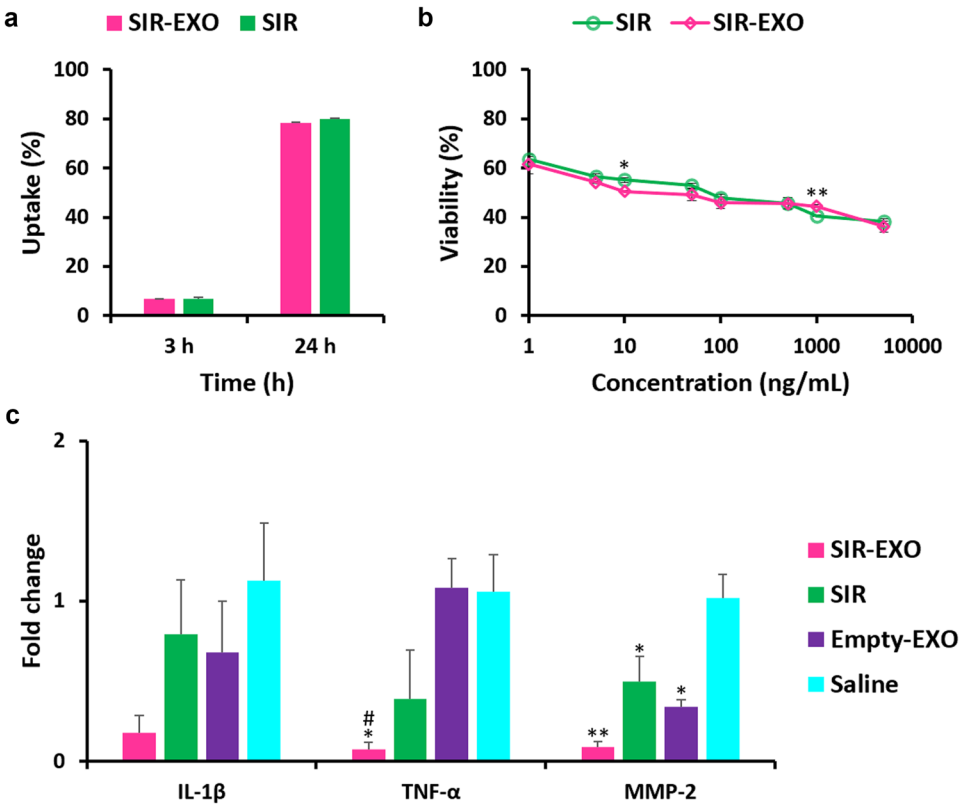

Fig. 5 **a** Cellular uptake results of drug suspension and SIR-EXO. **b** Cell viability data of drug suspension and SIR-EXO, $*p < 0.05$ and $**p < 0.01$. **c** Quantitative real-time PCR data obtained from different treatments, $*p < 0.05$ and $**p < 0.01$ compared with saline control and $\#p < 0.05$ compared to Empty-EXO group; data were reported as mean ± SEM, $n = 3$

of TNF-α and MMP-2 was 0.07 and 0.09 in the SIR-EXO treatment, compared to 1.06 and 1.02 in the saline control, respectively. Also, it can be observed that the drug suspension and Empty-EXO could not show comparable effects, and the nanodrug was significantly superior in this regard.

Moreover, SIR-EXO could successfully prevent the migration and invasion of SMCs in the scratch wound assay (Fig. 6). Soon after the scratching, SMCs started to migrate toward the established wound model, leading to the gradual wound closure (Fig. 6a). While both SIR and Empty-EXO showed a slight anti-migration effect, SIR-EXO significantly inhibited the SMCs' migration. At the endpoint of the experiment, SIR-EXO, SIR, and Empty-EXO exhibited 38, 61, and 73% wound closure, respectively, as compared to the mean of 88% closure in the saline control group (Fig. 6b).

Evaluation of SIR-EXO efficacy in the prevention of restenosis

Mechanical injury of arteries led to the formation of neointima and in vivo vascular imaging, pathological, and immunohistochemical analyses were carried out to assess the injury. CT angiography was applied as an in vivo 3D imaging method to validate the efficacy of SIR-EXO in a rat carotid injury model. The carotid artery undergone balloon angioplasty treated with SIR-EXO was observed acceptably open with normal blood flow compared to the control group (Fig. 7).

Further studies were performed on harvested carotid arteries and representative cross-sections stained by H&E were used for the calculation of neointimal area, N/M ratio, and stenosis percentage (Fig. 8). Anti-restenosis efficacy was observed in study groups in the following order: SIR-EXO > Empty-EXO > NS. N/M ratio was determined as 0.18, 0.81, and 1.91, and the stenosis percentages were about 5, 44, and 59 in SIR-EXO, Empty-EXO, and saline groups, respectively (Fig. 8b–d). Statistical analysis indicated that SIR-EXO significantly reduced stenosis compared to the NS group ($P < 0.001$) (Fig. 8d). Furthermore, Masson's trichrome and Orcein-Giemsa were used for staining collagen and elastic fibers, respectively. Different staining studies indicated the development of intimal hyperplasia in NS and Empty-EXO groups (Fig. 8).

Next, we investigated the expression of Ki67, α-SMA, and MMPs as markers for proliferation-activated fibrogenic SMCs, and inflammation, respectively [31–33]. Ki67- and α-SMA-positive cells played vital roles in the intimal hyperplasia since they were notably present in the control group (Fig. 9a). Obtained immunohistochemical images showed that SIR-EXO significantly decreased the expression of both markers compared with other studied groups suggesting that the proliferative and fibrogenic cells were suppressed successfully (Fig. 9a). Ki67 positive cells were 8%, 20%, and 37% of total

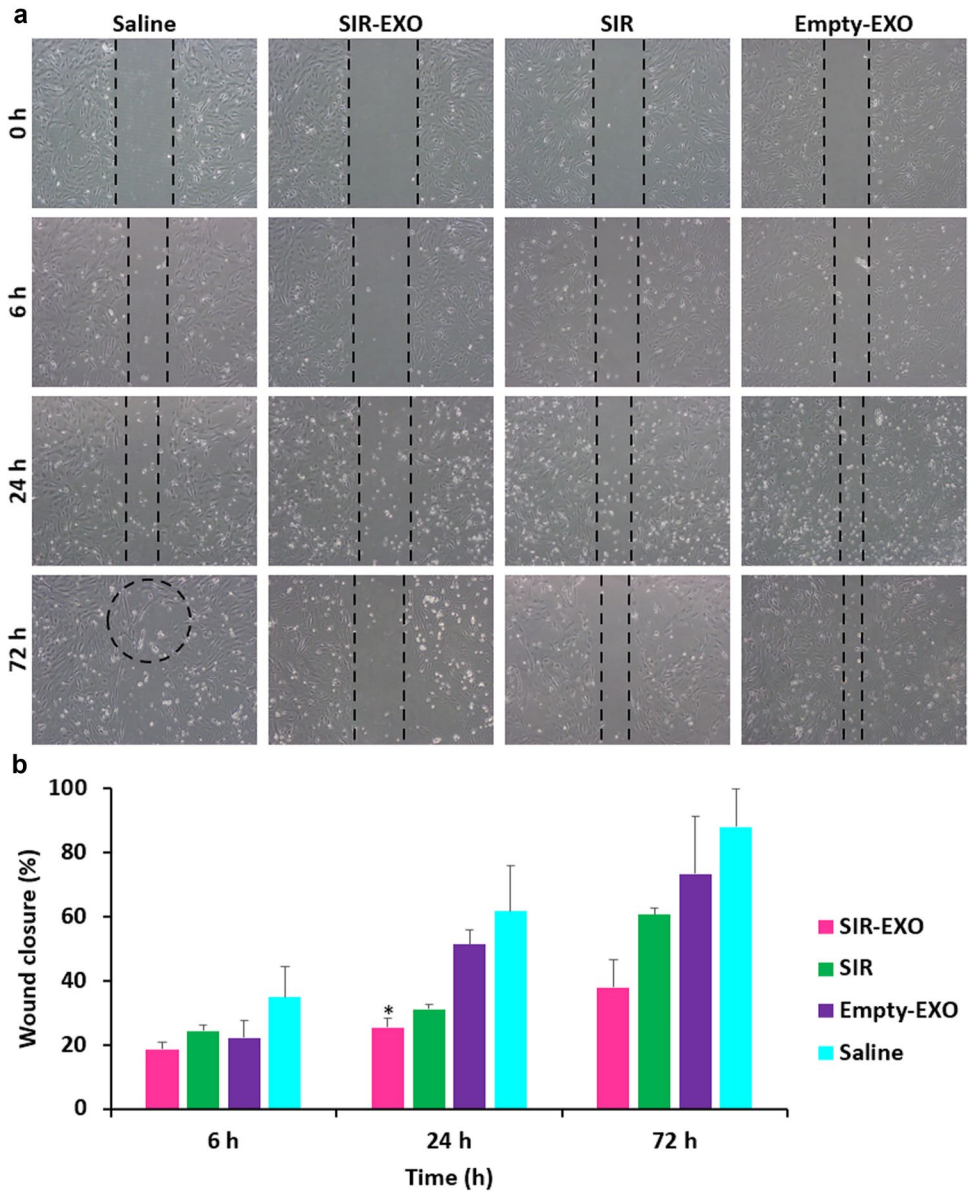

Fig. 6 **a** Representative microscopic images of wound healing assay at 0, 6, 24, and 72 h at 10 × magnification. **b** Quantified data of wound healing assay; data were reported as mean ± SEM, $n = 3$, $*p < 0.05$ compared with saline control

cells in the SIR-EXO, Empty-EXO, and saline groups, respectively (Fig. 9b). Also, quantified data demonstrated a decrease in α-SMA density resulting in the stained/total ratio of 0.11, 0.45, and 0.55 in these groups, respectively (Fig. 9c). MMPs are inflammatory mediators activated by different stimuli in vascular tissues [33]. According to Fig. 9d, SIR-EXOs and Empty-EXOs could slightly decrease the expression of MMP-2 and MMP-9, compared with the saline control.

Discussion

Balloon angioplasty is a common treatment in stenotic arteries, while post-intervention restenosis remains a major concern. Most studies revealed that migration and abnormal proliferation of media SMCs cause vascular restenosis in injured arteries. Also, denudation of vascular endothelium results in inflammatory responses that play a critical role in neointima formation. Therefore, anti-inflammatory and anti-proliferative drugs may be promising choices for the inhibition of restenosis [8, 34, 35]. Formerly, it was shown that local delivery of SIR in arteries significantly prevented restenosis [7]. SIR is a highly hydrophobic agent which cannot be prepared as an aqueous solution for administration via blood vessels. This limitation led to the application of nanocarriers for local SIR delivery [7, 36]. By this approach, Granada et al. introduced a novel porous balloon system containing sirolimus nanoparticles and showed its long-term and targeted efficacy in the porcine model of in-stent restenosis [37]. In another study, sirolimus polymeric nanoparticles

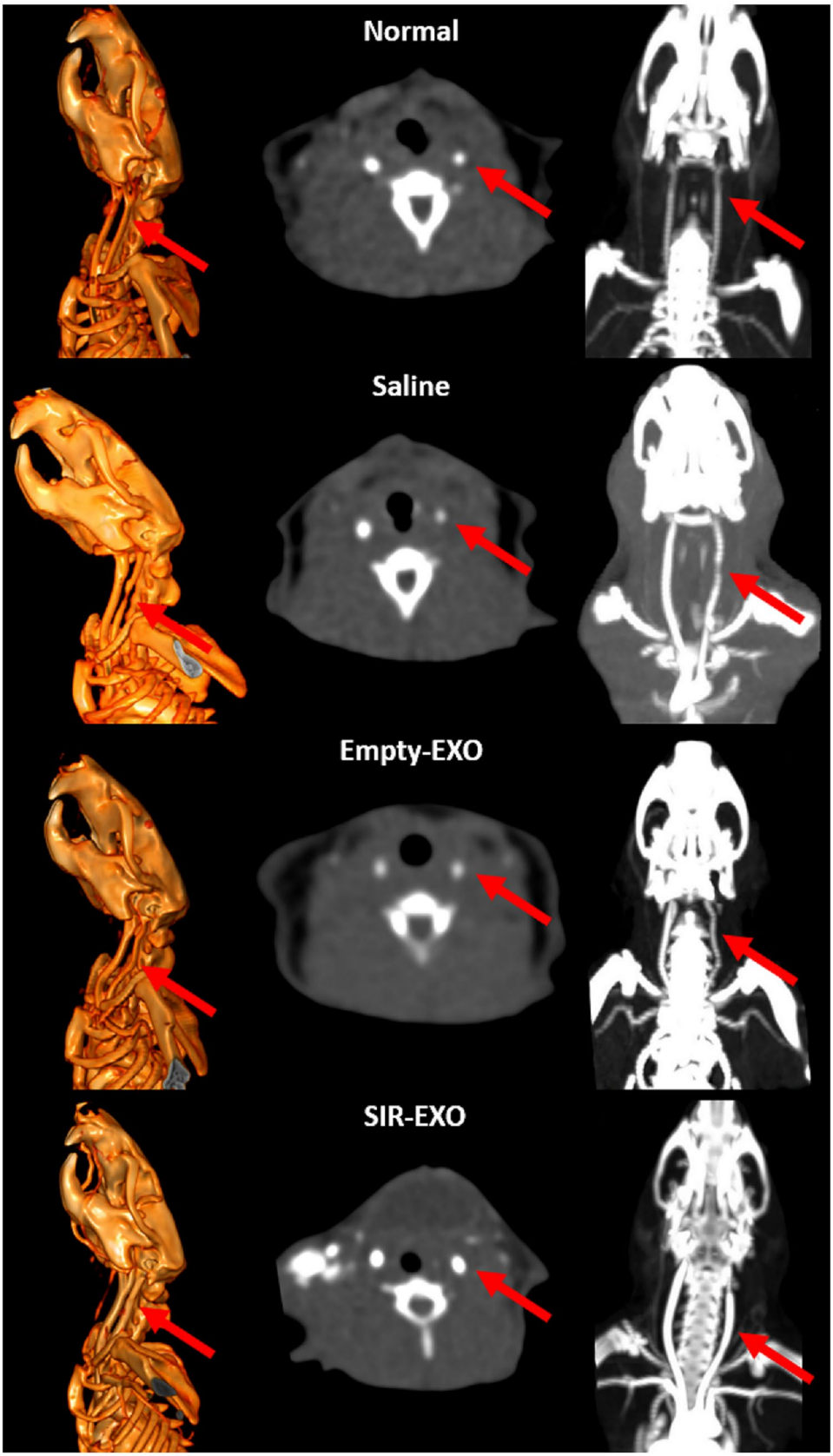

Fig. 7 In vivo imaging of rat carotid arteries; volume rendering reconstructions of animals, axial cross-sections of arteries, and maximum intensity projections

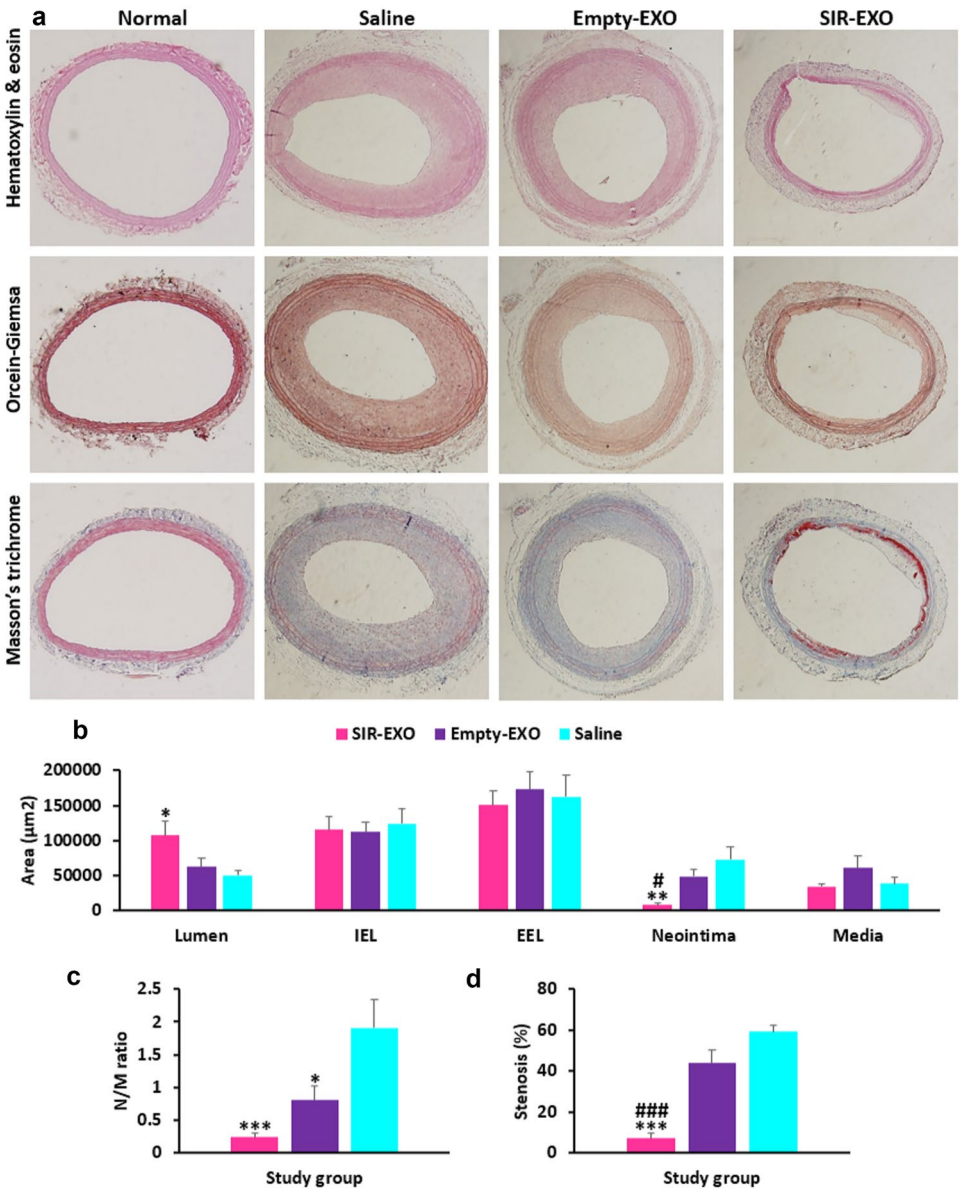

Fig. 8 **a** Cross-sections of harvested arteries from different study groups (SIR-EXO, Empty-EXO, saline, and normal) stained with H&E, Masson's trichrome, and Orcein-Giemsa. Quantitative morphometric analysis of carotid arteries. **b** Lumen, IEL, EEL, neointima, and media areas. **c** N/M ratio and **d** stenosis (%); all data were presented as mean ± SEM, $*p < 0.05$, $**p < 0.01$, and $***p < 0.001$ compared with saline control and $\#p < 0.05$, $\#\#\#p < 0.001$ compared to Empty-EXO group. Abbreviations: EEL external elastic lamina, IEL internal elastic lamina, N/M neointima/media

were used as a stent coating exhibiting considerable arterial permeation ex vivo [38].

Recently, exosomes have been introduced as a unique liposome-like drug delivery system with unique properties due to their rich cargo content [17, 20]. They serve as a biocompatible nanoplatform for the preparation of parenteral dosage forms of hydrophobic drugs, providing a prolonged release profile and diminished adverse effects [39, 40]. In the present study, we used the ultracentrifugation method for exosome purification from the culture medium of fibroblast cells. Ultracentrifugation is the most common method for the isolation of exosomes applied in pre-clinical studies [27].

Fibroblast cells were chosen as the exosome origin (Fig. 1) due to their stem cell-like properties and considerable scale-up potential [22, 41]. Furthermore, it was reported that fibroblast-derived exosomes carry the CD47 surface marker responsible for vesicle escape from phagocytosis [21, 40, 41]. Moreover, some recent studies applied human fibroblast extracellular vesicles (EVs) for collagen-replacement therapy [42] and wound healing [43] in mouse models and exhibited considerable therapeutic effects. In a recent study, dermal fibroblast-derived EVs were engineered to deliver anti-inflammatory payloads to the lung in a mouse model of acute lung injury which resulted in substantially reduced inflammation [44].

For the preparation of SIR-EXO, incubation was initially chosen as the loading method to protect the vesicular structure which is a major challenge of drug loading into exosomes [40, 45]. The incubation temperature was set at 37 °C to enhance the membrane fluidity. As

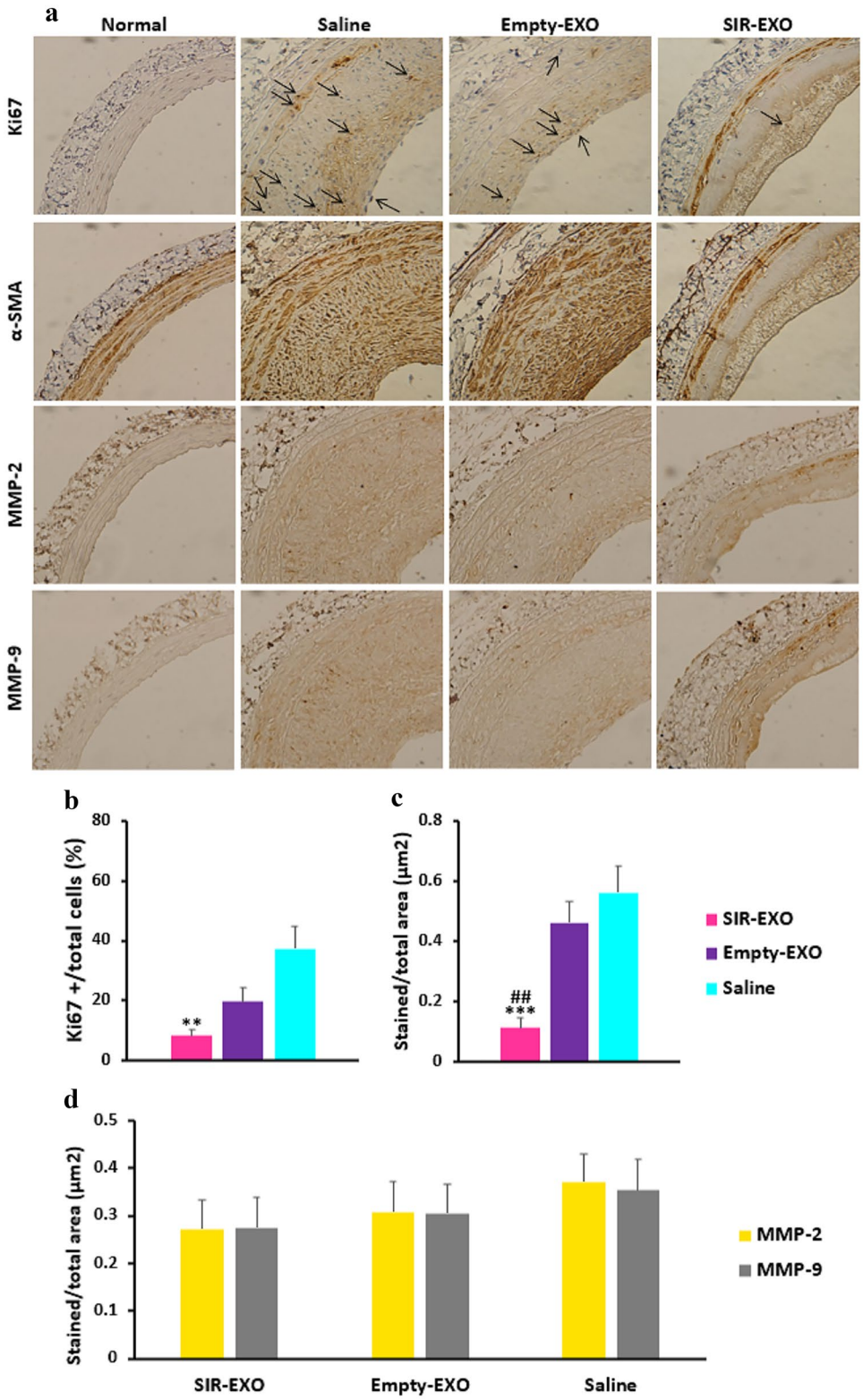

Fig. 9 **a** Ki67, α-SMA, MMP-2, and MMP-9 immunohistochemical staining of SIR-EXO, Empty-EXO, saline, and normal sections and quantified results of **b** Ki67, **c** α-SMA, and **d** MMPs in at least six randomly selected high power fields per group, All data were presented as mean ± SEM, $^{**}p < 0.01$, $^{***}p < 0.001$ compared to saline and $\#\#p < 0.01$ compared to Empty-EXO group

60-min incubation showed no significant increase in EE compared to 30-min incubation ($P > 0.05$), further loading studies were carried out on the shorter incubation period (Table 1). Additionally, electroporation and sonication could be applied to transiently permeabilize the bilayer membrane [40, 46]. Previous studies demonstrated improvement in the EE of both hydrophilic [47] and hydrophobic [39, 47] agents by applying these

techniques. Therefore, these procedures were added to simple incubation to increase EE but the results were not satisfying (Table 1).

As in most previous studies, the effect of the drug-to-exosome ratio has been disregarded, in the present study, we investigated three drug/protein ratios (2:1, 1:1, and 1:2), and the ratio of 1:2 resulted in a desirable EE. At a lower drug-to-exosome ratio, EE increased due to an increase in the number of vesicles and available bilayer space for SIR accommodation. The ratio of 1:2 was chosen for further loading investigation, and different modifications of the loading method showed no additional improvement indicating that nanocarriers may become saturated with SIR molecules through simple incubation (Table 1).

Loaded vesicles mostly exhibited an increase in mean diameter potentially as a result of SIR incorporation into the bilayer structure; however, zeta potential appeared to be close to empty vesicles with no major alteration (Table 1). Likewise, some previous studies reported a slight increase in the size of liposomes after SIR loading [48, 49]. Also, the optimized formulation of SIR-EXO was observed to have a round shape nanostructure similar to their vesicular structure before loading (Fig. 2a–c). Then, the presence of specific exosomal markers on loaded exosomes was verified by western blotting suggesting that the loading procedure had no destructive effects on the exosomal structure and surface proteins (Fig. 2d).

Optimum formulation (F6) was further studied regarding the release profile of SIR which may have a major impact on the formulation efficacy. SIR-EXO showed a desirable extended-release profile with an initial drug release probably due to leakage of surface-bound drug molecules which can provide a proper initial concentration in the first post-injury hours, followed by a sustained release of membrane-trapped drug molecules for several days potentially preventing late responses [50]. The lipidic membrane of exosomes acted like a depot for lipophilic SIR molecules leading to a prolonged release of about 50% of drug content during 3 weeks of the experiment (Fig. 3a). During the restenosis phenomenon, the initial inflammation peaks over the first 1–3 days, followed by a proliferative response peaking between 4 and 14 days, and the observed release profile might successfully prevent the responses [51].

Furthermore, the study of release kinetics demonstrated that the Higuchi model best describes the obtained release data. This model has been suggested for drug-loaded liposomes and contributed to a diffusion-controlled mechanism of drug release from nanostructures [29, 50, 52]. Moreover, the local pharmacokinetics determination and in vivo release data can provide a remarkable understanding of the efficacy timeline; however, the ethical consideration limited the number of animals in our research and should be the focus of future studies on intraarterial drug delivery studies.

FTIR analysis was applied for the understanding of interactions between drug molecules and exosomal structures. Therefore, characteristic peaks of SIR, Empty-EXO, and SIR-EXO were explored (Fig. 4a). In SIR spectrum, present peaks at 1454, 2873, 2933, and 2966 cm^{-1} correspond to macrocyclic groups of SIR molecules. Besides, 1649 and 3018 cm^{-1} peaks are associated with the triene group, and the peak at 1718 cm^{-1} represents carbonyl groups that were consistent with previous reports [25, 53]. FTIR spectrum of exosomes revealed a peak at 1072 cm^{-1} in the region related to phosphodiester groups of DNA and RNA. Furthermore, protein peaks are present between 1300 and 1800 cm^{-1}, and the peak observed at 1539 cm^{-1} is likely attributed to amide II of transmembrane proteins. The peak at 1398 cm^{-1} is related to CH bonds of acyl residues available in amines or lipids. The observed peak at 1745 cm^{-1} corresponds to C = O of cellular lipids and 2852 and 2922 cm^{-1} peaks are likely associated with CH vibrations of CH2 and CH3 in membranous fatty acids [54, 55]. It is worth noting that drug peaks were not recognizable in the loaded vehicles which may be due to the high exosome-to-drug ratio and covering SIR peaks. Also, there are no noticeable differences between spectra of empty and loaded exosomes implying that there were no major interactions between SIR molecules and exosomal components (Fig. 4a).

Previous studies on EVs suggested that exosomes may have anti-proliferate properties in several applications through different cellular pathways [56]. Furthermore, some recent studies have reported the application of exosomes for the inhibition of neointima hyperplasia [57–61]. Recently, the effects of exosomes originated from endothelial progenitor cells [57, 58], endothelial cells [58, 60], adipose mesenchymal stem cells [61], and human blood [59] were investigated on intimal formation. Some studies suggested that mechanisms involved in neointima formation may be altered by exosomes overexpressing TET2 [62] or containing miRNA-195 [60]. Gu et al. reported that 5-hydroxytryptamine transporter (5-HTT) expression was increased in injured arteries leading to the SMCs proliferation. This phenomenon was reversed using miRNA-195 containing exosomes originating from endothelial cells [60]. By another approach, Guan and colleagues suggested that the surface functionalization of stents by intact exosomes decreased adverse responses [59].

Besides, SIR was commonly applied for the prevention of restenosis [3, 7]. SIR acts against the proliferation and inflammatory responses and exhibited promising efficacy in the prevention of intimal formation in arteries undergoing angioplasty procedures [3, 24]. Considering the gradual formation of neointima, the active agent should be available at the target site for several days, and a sustained release delivery system serves as a desirable platform for this rationale [51, 63]. In this study, exosomes possessed a depot-like structure

for hydrophobic SIR. Furthermore, hemolysis tests approved the compatibility of SIR-EXO in the rat blood (Fig. 4b, c).

In the next step, the drug uptake was evaluated in SMCs as a main player in the restenosis phenomenon [34]. According to the similar cellular drug uptake of free SIR and SIR-EXO, it can be concluded that exosomes were successfully internalized by SMCs, and the cells were saturated with a specific amount of drug (Fig. 5a). Thereafter, the comparable viability profile of the SMCs treated by different concentrations of free SIR and SIR-EXO verified the antiproliferative efficacy of the nanodrug, compared to its free form (Fig. 5b). Similarly, another study showed significantly reduced viability in a < 10 ng/mL SIR dose and a steady viability profile in the range of 10–2500 ng/mL SIR in ESS-1 and MES-SA cell lines [64]. Recently, Asani et al. reported a dose-dependent reduced proliferation of pericytes treated by 5–1000 ng/mL SIR and a steady viability profile in the range of 1–15 µg/mL SIR [65].

In addition, the impact of SIR-EXO on the down-regulation of gene expression levels of IL-1β and TNF-α, as inflammation-related markers, and MMP-2, a migration marker, confirmed the anti-inflammation and migration properties of the formulation (Fig. 5c) [66]. Furthermore, the wound healing test was performed to functionally investigate the aforementioned effects of SIR-EXO on SMCs. As shown in Fig. 6, SIR-EXO treatment could considerably prevent the migration and invasion of SMCs, as compared to the saline control, SIR, and Empty-EXO.

The efficacy of exosomal SIR was investigated in a validated rat model of restenosis. As mentioned before, the post-angioplasty vascular injury was simulated, and the optimum formulation was then administered locally via a catheter. Unfortunately, the SIR solution could not be administered as the free drug control, due to the drug hydrophobicity and solvent limitations. After 2 weeks, the arteries were assessed by live imaging to be open with a normal blood flow (Fig. 7). According to obtained data, SIR-EXO and Empty-EXO treated groups demonstrated significant efficacy compared to the control groups. To verify CT imaging results, morphometric analyses of carotid artery sections were performed. Morphometric parameters revealed that SIR-EXO efficiently prevented stenotic responses. Arteries treated with SIR-EXO showed significantly diminished neointima formation, N/M ratio, and stenosis index (Fig. 8). It was reported that the nanoparticles of 100–200 nm could penetrate the artery wall and release their cargo resulting in the observed efficacy [67].

Furthermore, Ki67-positive cells were found to be less in the SIR-EXO group compared to other groups. Ki67, a proliferation marker expressed in different cell cycle phases except for G0 [32], was denser toward the neointima (Fig. 9a). Also, α-SMA expression as a marker of vascular contractility was consistent with Ki67 data and less expressed in the treatment group compared to the saline and Empty-EXO treated arteries (Fig. 9b, c) [31]. Similarly, the MMP-2 and MMP-9 were slightly less expressed in SIR-EXO carotids, compared to the saline control group (Fig. 9d). MMP-2 and MMP-9 facilitate the migration of vascular SMCs and regulate many signaling pathways involved in proliferation and apoptosis [33].

Conclusions

SIR-EXOs were prepared and optimized by studying different loading variables and then characterized regarding their structure and properties. The optimal formulation showed an extended-release profile of SIR appropriate for the prevention of arterial restenosis. According to obtained data, SIR-EXO were more efficacious in the inhibition of neointima formation compared to Empty-EXO and saline groups. Overall, it can be concluded that exosomes can serve as a promising drug delivery system for SIR and future studies may be focused on the complementary studies facilitating the introduction of SIR-EXO to the clinic and market.

Supplementary Information The online version contains supplementary material available at https://doi.org/10.1007/s13346-023-01390-z.

Acknowledgements The authors acknowledge support from Shahid Beheshti Medical University.

Author contribution Fatemeh Mehryab: investigation, methodology, formal analysis, visualization, writing—original draft, writing—review and editing. Shahram Rabbani: investigation, methodology, validation, resources, writing—review and editing. Faezeh Shekari: investigation, methodology, validation, resources, writing—review and editing. Abdoreza Nazari: investigation, methodology, writing—review and editing. Nazanin Goshtasbi: investigation, methodology, writing—review and editing. Azadeh Haeri: conceptualization, supervision, project administration, funding acquisition, resources, investigation, methodology, formal analysis, validation, visualization, writing—review and editing.

Funding This research was funded by the Iranian Council for Development of Stem Cell Sciences and Technologies (Vice-presidency for Science and Technology, Presidency of the Islamic Republic of Iran), grant number 11/38201 and Shahid Beheshti Medical University.

Availability of data and materials The datasets generated and/or analyzed during the current study are available from the corresponding author on reasonable request.

Declarations

Ethics approval The study was conducted according to the guidelines of the National Institutes of Health for the care and use of Laboratory Animals, and approved by the Ethics Committee of Shahid Beheshti University of Medical Sciences (protocol code IR.SBMU.PHARMACY.REC.1399.081 and date of approval 2020.06.16).

Consent to participate Not applicable.

Consent for publication Not applicable.

Competing interests The authors declare no competing interests.

References

1. Liu Y, Yang F, Zou S, Qu L. Rapamycin: a bacteria-derived immunosuppressant that has anti-atherosclerotic effects and its clinical application. Front Pharmacol. 2019;9:1520. https://doi.org/10.3389/fphar.2018.01520.
2. Onnis C, Cadeddu Dessalvi C, Cademartiri F, Muscogiuri G, Angius S, Contini F, et al. Quantitative and qualitative features of carotid and coronary atherosclerotic plaque among men and women. Front Cardiovasc Med. 2022;9:970438. https://doi.org/10.3389/fcvm.2022.970438.
3. Nestelberger T, Jeger R. Drug-coated balloons for small coronary vessel interventions: a literature review. Interv Cardiol (London, England). 2019;14(3):131–6. https://doi.org/10.15420/icr.2019.06.R3.
4. Andreou I, Stone PH, Ikonomidis I, Alexopoulos D, Sabate M. Recurrent atherosclerosis complications as a mechanism for stent failure. Hellenic J Cardiol. 2020;61(1):9–14. https://doi.org/10.1016/j.hjc.2019.04.007.
5. Cheng Y, Shibuya M, McGregor J, Conditt GB, Yi GH, Kaluza GL, et al. Biological effect on restenosis and vascular healing of encapsulated paclitaxel nanocrystals delivered via coated balloon technology in the familial hypercholesterolaemic swine model of in-stent restenosis. EuroIntervention. 2016;12(9):1164–73. https://doi.org/10.4244/eijv12i9a188.
6. Megaly M, Rofael M, Saad M, Shishehbor M, Brilakis ES. Outcomes with drug-coated balloons for treating the side branch of coronary bifurcation lesions. J Invasive Cardiol. 2018;30(11):393–9.
7. Haeri A, Sadeghian S, Rabbani S, Anvari MS, Ghassemi S, Radfar F, et al. Effective attenuation of vascular restenosis following local delivery of chitosan decorated sirolimus liposomes. Carbohyd Polym. 2017;157:1461–9. https://doi.org/10.1016/j.carbpol.2016.11.021.
8. Trepanier CM, Burke-Kleinman J, Strauss BH, Santerre JP, Bendeck MP. Less is more: developments in nanotechnology for antirestenosis therapies. Arterioscler Thromb Vasc Biol. 2023;43(7):1096–110. https://doi.org/10.1161/atvbaha.123.318450.
9. Haeri A, Sadeghian S, Rabbani S, Anvari MS, Lavasanifar A, Amini M, et al. Sirolimus-loaded stealth colloidal systems attenuate neointimal hyperplasia after balloon injury: a comparison of phospholipid micelles and liposomes. Int J Pharm. 2013;455(1–2):320–30. https://doi.org/10.1016/j.ijpharm.2013.07.003.
10. Akhlaghi S, Rabbani S, Alavi S, Alinaghi A, Radfar F, Dadashzadeh S, et al. Green formulation of curcumin loaded lipid-based nanoparticles as a novel carrier for inhibition of post-angioplasty restenosis. Mater Sci Eng: C. 2019;105:110037. https://doi.org/10.1016/j.msec.2019.110037.
11. Wang Y, Zhao D, Wei X, Ma L, Sheng J, Lu P. PEGylated polyethylenimine derivative-mediated local delivery of the shSmad3 inhibits intimal thickening after vascular injury. Biomed Res Int. 2019;2019:8483765. https://doi.org/10.1155/2019/8483765.
12. Sun Z, Yang J, Li H, Wang C, Fletcher C, Li J, et al. Progress in the research of nanomaterial-based exosome bioanalysis and exosome-based nanomaterials tumor therapy. Biomaterials. 2021;274:120873. https://doi.org/10.1016/j.biomaterials.2021.120873.
13. Bell BM, Kirk ID, Hiltbrunner S, Gabrielsson S, Bultema JJ. Designer exosomes as next-generation cancer immunotherapy. Nanomedicine: Nanotechnol Biol Med. 2016;12(1):163–9. https://doi.org/10.1016/j.nano.2015.09.011.
14. Montis C, Salvatore A, Valle F, Paolini L, Carlà F, Bergese P, et al. Biogenic supported lipid bilayers as a tool to investigate nano-bio interfaces. J Colloid Interface Sci. 2020;570:340–9. https://doi.org/10.1016/j.jcis.2020.03.014.
15. Thakur A, Parra DC, Motallebnejad P, Brocchi M, Chen HJ. Exosomes: Small vesicles with big roles in cancer, vaccine development, and therapeutics. Bioact Mater. 2022;10:281–94. https://doi.org/10.1016/j.bioactmat.2021.08.029.
16. Yang Z, Li Y, Wang Z. Recent advances in the application of mesenchymal stem cell-derived exosomes for cardiovascular and neurodegenerative disease therapies. Pharmaceutics. 2022;14(3):618.
17. Mehryab F, Taghizadeh F, Goshtasbi N, Merati F, Rabbani S, Haeri A. Exosomes as cutting-edge therapeutics in various biomedical applications: an update on engineering, delivery, and preclinical studies. Biochimie. 2023;213:139–67. https://doi.org/10.1016/j.biochi.2023.05.010.
18. Janockova J, Slovinska L, Harvanova D, Spakova T, Rosocha J. New therapeutic approaches of mesenchymal stem cells-derived exosomes. J Biomed Sci. 2021;28(1):39. https://doi.org/10.1186/s12929-021-00736-4.
19. Liao W, Du Y, Zhang C, Pan F, Yao Y, Zhang T, et al. Exosomes: the next generation of endogenous nanomaterials for advanced drug delivery and therapy. Acta Biomater. 2019;86:1–14. https://doi.org/10.1016/j.actbio.2018.12.045.
20. Mehryab F, Rabbani S, Shahhosseini S, Shekari F, Fatahi Y, Baharvand H, et al. Exosomes as a next-generation drug delivery system: an update on drug loading approaches, characterization, and clinical application challenges. Acta Biomater. 2020;113:42–62. https://doi.org/10.1016/j.actbio.2020.06.036.
21. Kamerkar S, LeBleu VS, Sugimoto H, Yang S, Ruivo CF, Melo SA, et al. Exosomes facilitate therapeutic targeting of oncogenic KRAS in pancreatic cancer. Nature. 2017;546(7659):498–503. https://doi.org/10.1038/nature22341.
22. Ichim TE, O'Heeron P, Kesari S. Fibroblasts as a practical alternative to mesenchymal stem cells. J Transl Med. 2018;16(1):212. https://doi.org/10.1186/s12967-018-1536-1.
23. Roskoski R Jr. Properties of FDA-approved small molecule protein kinase inhibitors: a 2020 update. Pharmacol Res. 2020;152:104609. https://doi.org/10.1016/j.phrs.2019.104609.
24. Freixo C, Ferreira V, Martins J, Almeida R, Caldeira D, Rosa M, et al. Efficacy and safety of sirolimus in the treatment of vascular anomalies: a systematic review. J Vasc Surg. 2020;71(1):318–27. https://doi.org/10.1016/j.jvs.2019.06.217.
25. Talimi R, Rabbani S, Mehryab F, Haeri A. Perivascular application of sirolimus multilayer nanofibrous mat for prevention of vascular stenosis: preparation, in vitro characterization, and in vivo efficacy evaluation. J Drug Deliv Sci Technol. 2022;77:103816. https://doi.org/10.1016/j.jddst.2022.103816.
26. Vahdat S, Pahlavan S, Mahmoudi E, Barekat M, Ansari H, Bakhshandeh B, et al. Expansion of human pluripotent stem cell-derived early cardiovascular progenitor cells by a cocktail of signaling factors. Sci Rep. 2019;9(1):16006. https://doi.org/10.1038/s41598-019-52516-8.
27. Thery C, Amigorena S, Raposo G, Clayton A. Isolation and characterization of exosomes from cell culture supernatants and biological fluids. Current protocols in cell biology. 2006; Chapter 3:Unit 3.22. https://doi.org/10.1002/0471143030.cb0322s30.
28. Mardpour S, Ghanian MH, Sadeghi-abandansari H, Mardpour S, Nazari A, Shekari F, et al. Hydrogel-mediated sustained systemic delivery of mesenchymal stem cell-derived extracellular vesicles improves hepatic regeneration in chronic liver failure. ACS Appl Mater Interfaces. 2019;11(41):37421–33. https://doi.org/10.1021/acsami.9b10126.
29. Jain A, Jain SK. In vitro release kinetics model fitting of liposomes: an insight. Chem Phys Lipid. 2016;201:28-40. https://doi.org/10.1016/j.chemphyslip.2016.10.005.

30. Javidi J, Haeri A, Shirazi FH, Kobarfard F, Dadashzadeh S. Synthesis, Characterization, in vivo imaging, hemolysis, and toxicity of hydrophilic Ag2S near-infrared quantum dots. J Cluster Sci. 2017;28(1):165–78. https://doi.org/10.1007/s10876-016-1060-5.
31. Hinz B, Celetta G, Tomasek JJ, Gabbiani G, Chaponnier C. Alpha-smooth muscle actin expression upregulates fibroblast contractile activity. Mol Biol Cell. 2001;12(9):2730–41. https://doi.org/10.1091/mbc.12.9.2730.
32. Gerdes J, Lemke H, Baisch H, Wacker HH, Schwab U, Stein H. Cell cycle analysis of a cell proliferation-associated human nuclear antigen defined by the monoclonal antibody Ki-67. J Immunol (Baltimore, Md : 1950). 1984;133(4):1710–5.
33. Chen Q, Jin M, Yang F, Zhu J, Xiao Q, Zhang L. Matrix metalloproteinases: inflammatory regulators of cell behaviors in vascular formation and remodeling. Mediator Inflamm. 2013;2013:928315. https://doi.org/10.1155/2013/928315.
34. Gallo G, Pierelli G, Forte M, Coluccia R, Volpe M, Rubattu S. Role of oxidative stress in the process of vascular remodeling following coronary revascularization. Int J Cardiol. 2018;268:27–33. https://doi.org/10.1016/j.ijcard.2018.05.046.
35. McDonald AI, Iruela-Arispe ML. Healing arterial ulcers: endothelial lining regeneration upon vascular denudation injury. Vascul Pharmacol. 2015;72:9–15. https://doi.org/10.1016/j.vph.2015.06.007.
36. Aqil F, Kausar H, Agrawal AK, Jeyabalan J, Kyakulaga AH, Munagala R, et al. Exosomal formulation enhances therapeutic response of celastrol against lung cancer. Exp Mol Pathol. 2016;101(1):12–21. https://doi.org/10.1016/j.yexmp.2016.05.013.
37. Granada JF, Tellez A, Baumbach WR, Bingham B, Keng YF, Wessler J, et al. In vivo delivery and long-term tissue retention of nano-encapsulated sirolimus using a novel porous balloon angioplasty system. EuroIntervention. 2016;12(6):740–7. https://doi.org/10.4244/eijy15m10_01.
38. Agrawal AA, Raval AJ, Velhal SM, Patel VV, Patravale VB. Nanoparticle-eluting stents for coronary intervention: formulation, characterization, and in vitro evaluation. Can J Physiol Pharmacol. 2022;100(3):220–33. https://doi.org/10.1139/cjpp-2021-0245.
39. Kim MS, Haney MJ, Zhao Y, Mahajan V, Deygen I, Klyachko NL, et al. Development of exosome-encapsulated paclitaxel to overcome MDR in cancer cells. Nanomed Nanotechnol Biol Med. 2016;12(3):655–64. https://doi.org/10.1016/j.nano.2015.10.012.
40. Kim MS, Haney MJ, Zhao Y, Yuan D, Deygen I, Klyachko NL, et al. Engineering macrophage-derived exosomes for targeted paclitaxel delivery to pulmonary metastases: in vitro and in vivo evaluations. Nanomed Nanotechnol Biol Med. 2018;14(1):195–204. https://doi.org/10.1016/j.nano.2017.09.011.
41. Mendt M, Kamerkar S, Sugimoto H, McAndrews KM, Wu CC, Gagea M et al. Generation and testing of clinical-grade exosomes for pancreatic cancer. JCI insight. 2018;3(8):e99263. https://doi.org/10.1172/jci.insight.99263.
42. You Y, Tian Y, Yang Z, Shi J, Kwak KJ, Tong Y, et al. Intradermally delivered mRNA-encapsulating extracellular vesicles for collagen-replacement therapy. Nat Biomed Eng. 2023;7(7):887–900. https://doi.org/10.1038/s41551-022-00989-w.
43. Gangadaran P, Oh EJ, Rajendran RL, Kim HM, Oh JM, Kwak S et al. Identification of angiogenic cargoes in human fibroblasts-derived extracellular vesicles and induction of wound healing. Pharmaceuticals (Basel). 2022;15(6):702. https://doi.org/10.3390/ph15060702.
44. Salazar-Puerta AI, Rincon-Benavides MA, Cuellar-Gaviria TZ, Aldana J, Vasquez Martinez G, Ortega-Pineda L et al. Engineered extracellular vesicles derived from dermal fibroblasts attenuate inflammation in a murine model of acute lung injury. Adv Mater. 2023;35(28):e2210579. https://doi.org/10.1002/adma.202210579.
45. Kalimuthu S, Gangadaran P, Rajendran RL, Zhu L, Oh JM, Lee HW, et al. A new approach for loading anticancer drugs into mesenchymal stem cell-derived exosome mimetics for cancer therapy. Front Pharmacol. 2018;9:1116. https://doi.org/10.3389/fphar.2018.01116.
46. Familtseva A, Jeremic N, Tyagi SC. Exosomes: cell-created drug delivery systems. Mol Cell Biochem. 2019;459(1–2):1–6. https://doi.org/10.1007/s11010-019-03545-4.
47. Fuhrmann G, Serio A, Mazo M, Nair R, Stevens MM. Active loading into extracellular vesicles significantly improves the cellular uptake and photodynamic effect of porphyrins. J Control Release. 2015;205:35–44. https://doi.org/10.1016/j.jconrel.2014.11.029.
48. Eloy JO, Petrilli R, Topan JF, Antonio HMR, Barcellos JPA, Chesca DL, et al. Co-loaded paclitaxel/rapamycin liposomes: development, characterization and in vitro and in vivo evaluation for breast cancer therapy. Colloids surf B biointerfaces. 2016;141:74–82. https://doi.org/10.1016/j.colsurfb.2016.01.032.
49. Onyesom I, Lamprou DA, Sygellou L, Owusu-Ware SK, Antonijevic M, Chowdhry BZ, et al. Sirolimus encapsulated liposomes for cancer therapy: physicochemical and mechanical characterization of sirolimus distribution within liposome bilayers. Mol Pharm. 2013;10(11):4281–93. https://doi.org/10.1021/mp400362v.
50. Haeri A, Sadeghian S, Rabbani S, Anvari MS, Boroumand MA, Dadashzadeh S. Use of remote film loading methodology to entrap sirolimus into liposomes: preparation, characterization and in vivo efficacy for treatment of restenosis. Int J Pharm. 2011;414(1–2):16–27. https://doi.org/10.1016/j.ijpharm.2011.04.055.
51. Schorn I, Malinoff H, Anderson S, Lecy C, Wang J, Giorgianni J, et al. The Lutonix® drug-coated balloon: a novel drug delivery technology for the treatment of vascular disease. Adv Drug Deliv Rev. 2017;112:78–87. https://doi.org/10.1016/j.addr.2017.05.015.
52. Ma J, Zhuang H, Zhuang Z, Lu Y, Xia R, Gan L, et al. Development of docetaxel liposome surface modified with CD133 aptamers for lung cancer targeting. Artif Cells Nanomed Biotechnol. 2018;46(8):1864–71. https://doi.org/10.1080/21691401.2017.1394874.
53. Stead SO, McInnes SJP, Kireta S, Rose PD, Jesudason S, Rojas-Canales D, et al. Manipulating human dendritic cell phenotype and function with targeted porous silicon nanoparticles. Biomaterials. 2018;155:92–102. https://doi.org/10.1016/j.biomaterials.2017.11.017.
54. Zlotogorski-Hurvitz A, Dekel BZ, Malonek D, Yahalom R, Vered M. FTIR-based spectrum of salivary exosomes coupled with computational-aided discriminating analysis in the diagnosis of oral cancer. J Cancer Res Clin Oncol. 2019;145(3):685–94. https://doi.org/10.1007/s00432-018-02827-6.
55. Baddela VS, Nayan V, Rani P, Onteru SK, Singh D. Physicochemical biomolecular insights into buffalo milk-derived nanovesicles. Appl Biochem Biotechnol. 2016;178(3):544–57. https://doi.org/10.1007/s12010-015-1893-7.
56. Bruno S, Collino F, Iavello A, Camussi G. Effects of mesenchymal stromal cell-derived extracellular vesicles on tumor growth. Front Immunol. 2014;5:382. https://doi.org/10.3389/fimmu.2014.00382.
57. Kong J, Wang F, Zhang J, Cui Y, Pan L, Zhang W, et al. Exosomes of endothelial progenitor cells inhibit neointima formation after carotid artery injury. J Surg Res. 2018;232:398–407. https://doi.org/10.1016/j.jss.2018.06.066.
58. Hu H, Jiang C, Li R, Zhao J. Comparison of endothelial cell- and endothelial progenitor cell-derived exosomes in promoting vascular endothelial cell repair. Int J Clin Exp Pathol. 2019;12(7):2793–800.
59. Hou YC, Li JA, Zhu SJ, Cao C, Tang JN, Zhang JY, et al. Tailoring of cardiovascular stent material surface by immobilizing exosomes for better pro-endothelialization function. Colloids surf B Biointerfaces. 2020;189:110831. https://doi.org/10.1016/j.colsurfb.2020.110831.

60. Gu J, Zhang H, Ji B, Jiang H, Zhao T, Jiang R, et al. Vesicle miR-195 derived from endothelial cells inhibits expression of serotonin transporter in vessel smooth muscle cells. Sci Rep. 2017;7:43546. https://doi.org/10.1038/srep43546.
61. Liu R, Shen H, Ma J, Sun L, Wei M. Extracellular vesicles derived from adipose mesenchymal stem cells regulate the phenotype of smooth muscle cells to limit intimal hyperplasia. Cardiovasc Drugs Ther. 2016;30(2):111–8. https://doi.org/10.1007/s10557-015-6630-5.
62. Li B, Zang G, Zhong W, Chen R, Zhang Y, Yang P, et al. Activation of CD137 signaling promotes neointimal formation by attenuating TET2 and transferrring from endothelial cell-derived exosomes to vascular smooth muscle cells. Biomed Pharmacother. 2020;121:109593. https://doi.org/10.1016/j.biopha.2019.109593.
63. Schiener M, Hossann M, Viola JR, Ortega-Gomez A, Weber C, Lauber K, et al. Nanomedicine-based strategies for treatment of atherosclerosis. Trends Mol Med. 2014;20(5):271–81. https://doi.org/10.1016/j.molmed.2013.12.001.
64. Bobiński M, Okła K, Łuszczki J, Bednarek W, Wawruszak A, Moreno-Bueno G, et al. Gemcitabine and selected mTOR inhibitors in uterine sarcomas and carcinosarcoma cells- an isobolographic analysis. Int J Med Sci. 2020;17(18):2987–97. https://doi.org/10.7150/ijms.48187.
65. Asani B, Siedlecki J, Wertheimer C, Liegl R, Wolf A, Ohlmann A, et al. Anti-angiogenic properties of rapamycin on human retinal pericytes in an in vitro model of neovascular AMD via inhibition of the mTOR pathway. BMC Ophthalmol. 2022;22(1):138. https://doi.org/10.1186/s12886-022-02334-w.
66. Zha Y, Yang Y, Zhou Y, Ye B, Li H, Liang J. Dietary evodiamine inhibits atherosclerosis-associated changes in vascular smooth muscle cells. Int J Mol Sci. 2023;24(7):6653. https://doi.org/10.3390/ijms24076653.
67. Westedt U, Barbu-Tudoran L, Schaper AK, Kalinowski M, Alfke H, Kissel T. Deposition of nanoparticles in the arterial vessel by porous balloon catheters: localization by confocal laser scanning microscopy and transmission electron microscopy. AAPS PharmSci. 2002;4(4):E41. https://doi.org/10.1208/ps040441.